Confinement of Half-quantized Vortices in Coherently Coupled Bose–Einstein Condensates: Simulating Quark Confinement in QCD

Minoru Eto[1], Muneto Nitta[2]
[1]*Department of Physics, Yamagata University, Kojirakawa-machi 1-4-12, Yamagata, Yamagata 990-8560, Japan,*
[2]*Department of Physics, and Research and Education Center for Natural Sciences, Keio University, Hiyoshi 4-1-1, Yokohama, Kanagawa 223-8521, Japan*

(Dated: February 17, 2017)

We demonstrate that the confinement of half-quantized vortices (HQVs) in coherently coupled Bose–Einstein condensates (BECs) simulates certain aspects of the confinement in $SU(2)$ quantum chromodynamics (QCD) in 2+1 space-time dimensions. By identifying the circulation of superfluid velocity as the baryon number and the relative phase between two components as a dual gluon, we identify HQVs in a single component as electrically charged particles with a half baryon number. Further, we show that only singlet states of the relative phase of two components can stably exist as bound states of vortices, that is, a pair of vortices in each component (a baryon) and a pair of a vortex and an antivortex in the same component (a meson). We then study the dynamics of a baryon and meson; baryon is static at the equilibrium and rotates once it deviates from the equilibrium, while a meson moves with constant velocity. For both baryon and meson we verify a linear confinement and determine that they are broken, thus creating other baryons or mesons in the middle when two constituent vortices are separated by more than some critical distance, resembling QCD.

arXiv:1702.04892v1 [cond-mat.quant-gas] 16 Feb 2017

I. INTRODUCTION

In modern elementary particle physics, one of the most important and difficult problems is the confinement of quarks (and gluons) in quantum chromodynamics (QCD). What we daily observe in nature at low energy are not elementary constituents, that is, quarks and gluons but they are strongly confined to form hadrons. There are two types of hadrons: baryons, consisting of only quarks, and mesons, consisting of quarks and antiquarks. Various baryons and mesons can exist because there are several species (called as flavors) of quarks, such as up (u) and down (d). The widely accepted explanation of the confinement is that chromo-electric flux from a quark is squeezed to form a flux tube in a dual superconductor, in which magnetic monopoles are condensed [1–3]. Thus, the interaction energy between (anti-)quarks is proportional to the distance between them; this is a salient signal of the confinement. Although the explanation is quite plausible, it is difficult to prove it. Therefore, many studies have been conducted for QCD-like theories.

From among these studies, Polyakov [4] made an important remark using a duality about a $U(1)$ gauge theory in 2+1 space-time dimensions; this can be obtained as the low-energy limit of an $SU(2)$ gauge theory with a triplet scalar field. The duality mentioned here is the one between the XY and Abelian–Higgs models in $2+1$ dimensions [5, 6], providing insights for understanding the fractional quantum Hall effect [7], Mott transitions [8], etc. As a photon has only one polarization in three spece-time dimensions, it can be dualized to the so-called dual photon (a periodic scalar field) $\theta \in [0, 2\pi)$ defined through $\partial_\mu A_\nu - \partial_\nu A_\mu = \frac{g_c^2}{4\pi}\varepsilon_{\mu\nu\rho}\partial^\rho\theta$ with a coupling g_c. Under the duality relation, electrically charged bosons in the original theory are interchanged by vortices in θ. The dual photon is massless in the perturbation theory but it gets mass $m_{\rm dp}$ through nonperturbative monopole effects, and is consequently described at low energy by the Lagrangian

$$\mathcal{L}_{\rm dp} = \frac{g_c^2}{32\pi^2}\partial_\mu\theta\partial^\mu\theta + cg_c^2 m_{\rm dp}^2\cos\theta \tag{1}$$

where c is a constant. Clearly, a θ vortex must be attached by a soliton because of the potential term, which corresponds to an electric flux tube in the original theory showing confinement.

In this work, we show that this confinement phenomenon can be simulated in ultracold atomic gases of coherently coupled two-component BECs, which is an experimentally controllable ideal system [9–11], as realized by the JILA group [12, 13]. In particular, quantized vortices in ultracold atomic BECs have been studied thoroughly since their experimental realization [14]. The recent progress in this subject can be seen in the development of techniques to nucleate the vortices and detect real-time vortex dynamics [15]. Theoretically, they are described by the Gross–Pitaevskii (GP) equations:

$$\left[i\hbar\frac{\partial}{\partial t} + \frac{\hbar^2}{2m}\nabla^2 - \left(g_i|\Psi_i|^2 + g_{12}|\Psi_{\hat{i}}|^2 - \mu_i\right)\right]\Psi_i = -\hbar\omega\Psi_{\hat{i}}\,, \tag{2}$$

where $\hat{1} = 2$, $\hat{2} = 1$, g_{ij} represents the atom–atom coupling constants, m is the mass of atom, and μ_i represents the chemical potential. The first and second condensates $\Psi_{1,2}$ are coherently coupled through the Rabi (Josephson) terms with the Rabi frequency ω. Such coherent coupling was achieved by the JILA group [13].

In the following, we assume $g_1 = g_2 = g$ and $\mu_1 = \mu_2$ for simplicity, and focus on a miscible BEC ($g > g_{12}$) in which both condensates coexist as $v = |\Psi_1| = |\Psi_2| = \sqrt{(\mu+\hbar\omega)/(g+g_{12})}$. The system has the symmetry $[U(1)_S \times U(1)_R]/\mathbb{Z}_2$: $(\Psi_1, \Psi_2) \to (e^{i\alpha}\Psi_1, e^{\pm i\alpha}\Psi_2)$, where $+$ is for $U(1)_S$ and $-$ is for $U(1)_R$. The Lagrangian for Eq. (2) is

$$\mathcal{L}_{\rm GP} = \sum_i \Big[-\frac{i\hbar}{2}\left(\Psi_i\dot{\Psi}_i^* - \dot{\Psi}_i\Psi_i^*\right) - \frac{\hbar^2}{2m}|\nabla\Psi_i|^2 + \mu_i|\Psi_i|^2 - \frac{g_i}{2}|\Psi_i|^4\Big] - g_{12}|\Psi_1\Psi_2|^2 - V_R, \quad (3)$$

where $V_{\rm R} = -\hbar\omega\,(\Psi_1\Psi_2^* + \Psi_1^*\Psi_2)$. We then truncate this by substituting the expression of the condensates $\Psi_i = (v + r_i)e^{i\theta_i}$ into Eq. (3) and by integrating out the amplitudes r_i:

$$\tilde{\mathcal{L}}_{\rm GP} = \frac{\hbar^2}{4(g+g_{12})}\dot{\theta}_+^2 + \frac{\hbar^2}{4(g-g_{12})}\dot{\theta}_-^2 - \frac{\hbar^2 v^2}{4m}(\nabla\theta_+)^2 - \frac{\hbar^2 v^2}{4m}(\nabla\theta_-)^2 + 2\hbar\omega v^2\cos\theta_-, \quad (4)$$

where we ignored constants and managed the Rabi term perturbatively. Here, $\theta_+ \equiv \theta_1 + \theta_2$ is a phonon and $\theta_- \equiv \theta_1 - \theta_2$ is known as the Leggett mode or phason, corresponding to θ in Eq. (1). The superfluid velocity is $\mathbf{v}_{\rm s} = \frac{\hbar}{m}\nabla\frac{\theta_1+\theta_2}{2}$, and vortex winding number is defined by $N_B = \frac{m}{\hbar}\oint_C d\mathbf{s}\cdot\mathbf{v}_{\rm s} = \frac{n_1+n_2}{2}$, where C is a closed path enclosing all the vortices, and $n_i \in \mathbb{Z}$. In the miscible ground state, vortices winding in θ_1 and θ_2 are half-quantized vortices (HQVs); this significantly differs from the simpler model in Eq. (1). HQVs have been observed recently [17]. Our proposal is to identify the winding number N_B as a baryon number in $SU(2)$ QCD, and HQVs winding in θ_1 and θ_2 as u (up) and d (down) (bosonic) quarks, respectively. Previous studies suggested [16] and confirmed [18, 19] that u- and d-vortices are connected through a soliton resembling the confinement (see also [20–22]). In Ref. [23], a similarity based on disintegration of confining strings between HQVs was pointed out. In the current study, we show that all stable bound states of vortices are singlet states of $U(1)_R$, that is, a baryon ud and mesons $\bar{u}u$ and $\bar{d}d$. We further identify $U(1)_R$ as a dual gluon (the diagonal component of $SU(2)$ color symmetry). We then achieve a fine agreement with $SU(2)$ QCD for which confinement allows only singlet states of $SU(2)$. We further numerically simulate the disintegration of solitons in baryon and meson when constituents are separated, as in the QCD case.

II. CONFINEMENT

a. Liberated vortices The static intervortex forces between the well-separated unconfined HQVs ($\omega = 0$) at distance R were found [24] as $\frac{U_{uu}}{U_*} = -\frac{2}{\pi}\log\rho$ and $\frac{U_{ud}}{U_*} = \frac{\pi}{2}\frac{g_{12}}{g-g_{12}}\frac{1}{\rho^2}\log\frac{\rho}{\xi}$, with $U_* = v^2\hbar^2/m$, $R_* = \sqrt{2\hbar^2/\mu m}$, $\rho = R/R_*$, and ξ is a dimensionless constant. The interactions between other pairs are $U_{uu} = U_{dd} = -U_{\bar{u}u} = -U_{\bar{d}d}$ and $U_{ud} = U_{\bar{u}d} = U_{\bar{d}u} = U_{\bar{u}\bar{d}}$. Therefore, irrespective of the sign of the coupling constants g and g_{12}, $U_{uu,dd}$ is repulsive while $U_{u\bar{u},d\bar{d}}$ is attractive. They are nothing but the 2+1 dimensional Coulomb potentials. In contrast, the potentials between the different species are blind to whether they are vortex or antivortex, and are always repulsive (attractive) for $g_{12} > 0$ ($g_{12} < 0$).

By applying the point particle approximation to Eq. (2) [25], we can derive $\frac{dZ_i}{d\tau} = -\frac{i}{\pi q_i}\frac{\partial}{\partial\bar{Z}_i}\frac{U}{U_*}$, where $Z_i(\tau) = X_i(\tau) + iY_i(\tau)$ is the position of the i-th vortex in terms of the dimensionless coordinates $\tau = \mu t/2\hbar$ and $\vec{y} = \vec{x}/R_*$, and U is either of the $U_{\bar{u}u}$ or U_{ud} type according to components of the pair. We use the dimensionless coupling $u = 2g/\mu$, $u_{12} = 2g_{12}/\mu$, and $\eta = 2\hbar\omega/\mu$ in the following. As U depends only on $R/R_* = |Z_1 - Z_2|$, this can be easily solved: Each component of the uu (dd) pair rotates the other counterclockwise, while the pair ud rotates counterclockwise (clockwise) for $u_{12} > 0$ ($u_{12} < 0$). As $U_{uu} \sim \log R$ is much greater than $U_{ud} \sim (\log R)/R^2$, uu (dd) rotates quicker than ud. The other pairs, $\bar{u}u$, $\bar{d}d$, $\bar{u}d$, and $\bar{d}u$ show linear and parallel motions, with the distance R being preserved.

b. Confined vortices When $\omega \neq 0$, $U(1)_R$ is explicitly broken, metastable sine-Gordon soliton appears which is also called as a magnetic domain wall [22, 26–28]. The solution and its tension are given as $\theta_- = 4\arctan\exp\sqrt{\frac{2m\omega}{\hbar}}\,x$, and $T_{\rm SG} = 8v^2\frac{\hbar^2}{m}\sqrt{\frac{m\omega}{\hbar}}$, respectively. This confines the constituent vortices, so that only $U(1)_R$ singlet composite states (a baryon ud with $N_B = 1$ and a meson $\bar{u}u$ (or $\bar{d}d$) with $N_B = 0$) must remain stable as in QCD. The remaining pairs, uu, dd, $\bar{u}d$, and $\bar{d}u$, which are not $U(1)_R$ singlets, should not appear [29].

In addition to the intervortex potentials $U_{ud,\bar{u}u}$, the linear confining potential $U_{\rm SG} = T_{\rm SG}R$ contributes to the vortex dynamics. However, note that $U_{\rm SG} = T_{\rm SG}R$ is an approximation, which is obtained under the assumption that $|\Psi_i| = v$ holds everywhere. Therefore, we should correct the soliton tension appearing inside the baryons and mesons. Hence, we applied the imaginary time $\tilde{t}$ evolution method to an initial configuration made by simply superposing two unconfined vortex solutions ($\omega = 0$) with a large initial distance $R = 60R_*$. Fig. 1(a) plots the static total mass M from Eq. (3) as a function of molecule size $R(\tilde{t})$. Initially, M rapidly decreases because of a large deformation in the condensate profiles, while the molecule size remains almost unchanged. After a while, the mass reduction moderates and the imaginary evolution slows. At that instance, the function $M(R)$ exhibits linear behaviors, as shown in Fig. 1(a). The tension of a soliton is presented by the slope of the linear behavior. We numerically confirmed that the tension is smaller than $T_{\rm SG}$ by approximately 10%–20%, and the

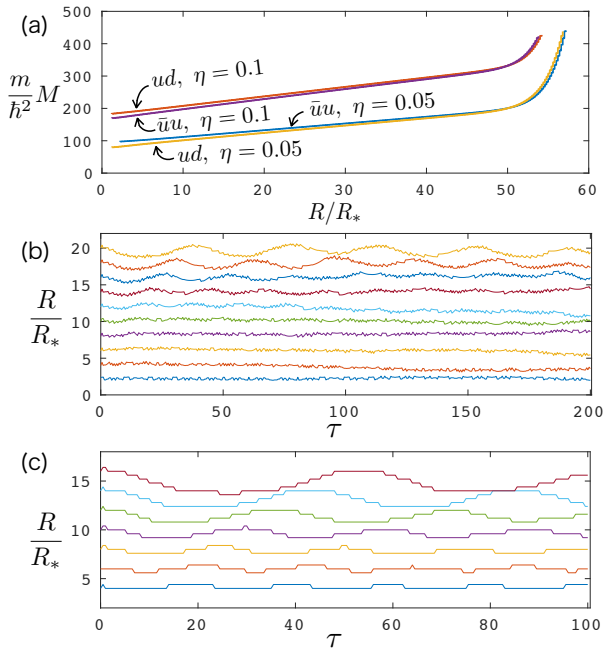

FIG. 1. (a) Mass M of a molecule of size R under the relaxation process with initial separation is $60R_*$. The four cases are shown for the meson $\bar{u}u$ and baryon ud with $\eta = 0.05$ and 0.1. Fluctuations of the baryon (b) and the meson (c) are shown under the real time evolution. The couplings are chosen as $u = 2u_{12} = 1$.

correct confining potential is

$$U_{\rm conf} = \alpha T_{\rm SG} R = 8\alpha U_* \sqrt{\eta}\,\rho. \tag{5}$$

For example, according to Fig. 1(a), $\alpha = 0.85$ for ud while $\alpha = 0.88$ for $\bar{u}u$, with $\eta = 0.1$.

Let us next turn to real time dynamics. Our initial configurations are obtained as a result of the imaginary time evolution with sufficiently long duration until at least the configuration reaches the linear line, as shown in Fig. 1(a). With this configuration as the initial configuration, we switch on the real time evolution. The baryon ud for $u_{12} > 0$ is static at an equilibrium where the repulsive intervortex force is balanced with the soliton's attractive force. Once the distance R is deviated from the equilibrium distance R_0, the interaction is repulsive (attractive) for $R < R_0$ ($R > R_0$), thus causing the baryon to rotate. By numerically solving GP equations (2) we confirmed that the baryon of $R < R_0$ rotates counterclockwise while that of $R > R_0$ rotates clockwise. See Appendix A and the movies in Ancillary files for details of the numerical solutions to the GP equations. This can also be explained by the point particle approximation explained earlier that included the confining potential $U_{\rm conf}$. The total effective potential $U_{\rm tot} = U_{ud} + U_{\rm conf}$ remains a function on R only so that it can be solved easily. The ud molecule rotates (counter)clockwise when $U_{\rm tot}$ is attractive (repulsive) with constant period $\mathcal{T} = 2\pi^2\rho\left(\frac{\partial}{\partial\rho}\frac{U_{\rm tot}}{U_*}\right)^{-1}$.

This works similarly for the mesons by replacing U_{ud} by $U_{\bar{u}u}$. They linearly move with a constant velocity $\mathcal{V} = \frac{1}{2\pi}\frac{\partial}{\partial\rho}\frac{U_{\rm tot}}{U_*}$. The effect of the soliton can be most clearly seen when the separation is large where $\mathcal{T}$ and $\mathcal{V}$ asymptotically behave as

$$\mathcal{T} \to \frac{\pi^2}{4\alpha\sqrt{\eta}}\rho, \qquad \mathcal{V} \to \frac{8\alpha\sqrt{\eta}}{\pi}, \qquad (R \gg R_*)\,. \tag{6}$$

We confirmed these asymptotic behaviors by numerically solving the GP equation. α can be determined from Eq. (6), for example $\alpha = 0.85$ for $\eta = 0.1$ baryon, which is consistent with the result from the imaginary time evolution in Eq. (5).

III. FRAGMENTATION OF SOLITON

When a molecule is elongated beyond a critical length R_c, the soliton will break up into small pieces. While approaching to the critical size R_c from a depressed size, the molecule starts to oscillate, and the instability develops toward fragmentation. We plot the molecule size as a function of time in Fig. 1(b) and (c), which show that the larger molecule has larger amplitude in the oscillational mode. Fig. 2 shows the molecule fragments when its size reaches R_c. As $T_{\rm SG}$ is proportional to $\sqrt{\eta}$, R_c recueces

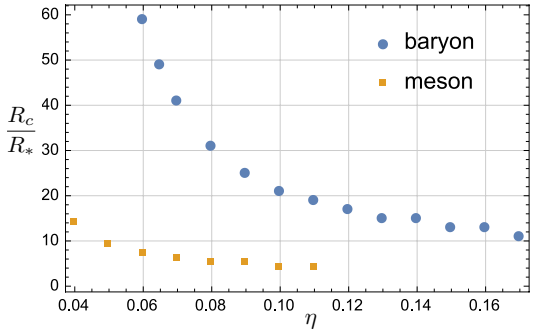

FIG. 2. Relations between η and the critical molecule size R_c at which fragmentation occurs for $u = 2u_{12} = 1$.

(enlarges) for a large (small) η. As both $U_{\bar{u}u}$ and $U_{\rm conf}$ are attractive for the meson, R_c for the meson is smaller than that for the baryon for $u_{12} > 0$.

The disintegration of a baryonic molecule in a harmonic trapping potential was reported in Ref. [23]. In the current study, we investigated both baryons and mesons. In contrast to in findings in [23] ($u_{12} = 0$), we consider $u_{12} > 0$ and a homogeneous system without a trapping potential to exclude external effects from environment and focus on consequences purely due to confinement.

a. Baryonic molecule We conducted numerous simulations for various initial molecule sizes $R_{\rm ini}$. To provide a bench-mark, we set $\eta = 0.1$ with the equilibrium length $R_0 = 0.66R_*$ and critical length $R_c \simeq 21R_*$. We set $R_{\rm ini}$ much larger than R_0. ud rotates as if it

is a solid stick when its size is not extremely large, for example, $R_{\rm ini} = 8R_*$. When we further enlarge the molecule ($R_{\rm ini} = 20R_*$), though ud does not break up, the soliton starts twisting sideways. When $R_{\rm ini}$ becomes larger than the critical value $R_{\rm c}$, fragmentation occurs for $R_{\rm ini} = 24R_*$, as shown in Fig. 3.

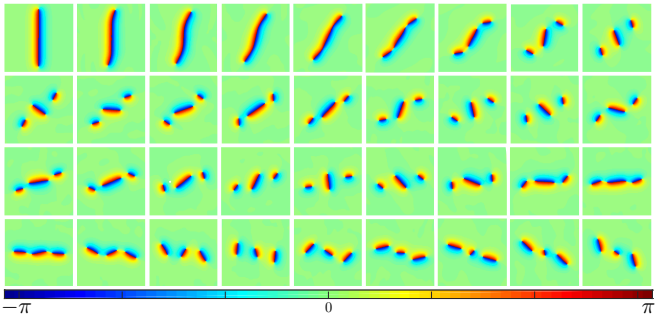

FIG. 3. Motion of a ud baryon ($\tau = 0$ - 175 with a step $\Delta\tau = 5$) with $R_{\rm ini}/R_* = 24$. θ_- is plotted. The spatial region $\vec{y} \in [-15, 15]^2$ is shown. $u = 2u_{12} = 10\eta = 1$.

In detail, the fragmentation occurs as follows. The u and d vortices at the edges rotate rapidly with the period given in the asymptotic formula (6); however, the long soliton maintains its initial position. As a result, a large gap emerges between the rotation speed of soliton near the edge and center. This causes the soliton to curve and break up. The fragmentation always occurs at points near the edges. After short baryons are released from the edge, an antibaryon remains at the center. As shown in Fig. 3, the two baryons at the outer sides rotate clockwise, and simultaneously revolve clockwise. The revolution speed of the two outer baryons is much slower than the rotation speed of a long original baryon before breaking up. This is because after the fragmentation, the two short baryons at outer sides are no longer connected by the soliton, reducing the interaction, and therefore the rotation speed is very small. However, the antibaryon at the center rotates counterclockwise. Interestingly, the lengths of baryon and antibaryon oscillate from time to time. If we place an even longer baryon initially, it splits up into smaller pieces, see Appendix A.

b. Mesonic molecule For concreteness, we again set $\eta = 0.1$. We initially prepared $\bar{u}u$. A short meson runs downward with a constant speed as a solid stick. A slightly longer meson, shown in the panels of the line Fig. 4(a) for $R_{\rm ini}/R_* = 16$ breaks up into a pair of baryon and antibaryon by creating $\bar{d}$ and d at the middle, as $\bar{u}u \to \bar{u}\bar{d} + du$. The pair continues to run straight downward as $\bar{u}\bar{d}$ and du can be seen as a pair of integer vortex and antivortex, respectively, while they rotate oppositely. After a while, when they rotate by 180°, they fuse again and become another type of meson, namely $\bar{d}d$. The meson repeats this exchange $\bar{u}u \leftrightarrow \bar{d}d$. Interestingly, this suggests that the actual meson state is $\bar{u}u \pm \bar{d}d$ (in a long period), as in QCD. The longer $\bar{u}u$ meson ($R/R_* = 22$),

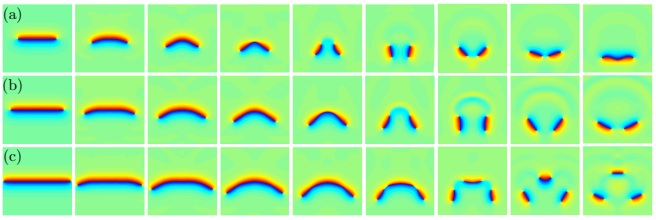

FIG. 4. (a)-(c) Motions of a meson ($\tau = 0$ - 40 with a step $\Delta\tau = 5$) with $R_{\rm ini}/R_* = 16, 22, 28$, respectively. See the caption of Fig. 3 for the parameters.

as shown in panels of the line Fig. 4(b), also fragments and changes as $\bar{u}u \to \bar{u}\bar{d} + du$. Unlike case (a), du and $\bar{u}\bar{d}$ do not coalesce, and an up-going rarefaction pulse is emitted. The pair of baryon and antibaryon rotate oppositely and run downward. A very long meson with $R/R_* = 28$, shown in panels of the line Fig. 4(c), is quite similar to that in case (b), except that it now emits another meson instead of a rarefaction pulse. The initial meson breaks up into three pieces as $\bar{u}u \to \bar{u}\bar{d} + d\bar{d} + du$. The created meson at the middle is $d\bar{d}$ not $\bar{d}d$; therefore, it runs upward. If we prepare a much longer meson initially, it will break up into larger number of small molecules, see Appendix A and movies in Ancillary files.

IV. CONCLUDING REMARKS

In this work, we studied the real time dynamics and confinement of baryonic and mesonic vortex molecules in coherently coupled two-component BECs in 2+1 dimensions. We observed that only $U(1)_R$ singlet states of vortex bound states can appear linearly confined by solitons, thereby simulating QCD. In addition, we numerically showed that a short baryon rotates and a short meson moves straight; this can be accounted well by the point vortex approximation, whereas molecules longer than R_c involve fragmentation. The disintegration of mesons includes rich phenomena, that is, a meson transitioning into a pair of a baryon and an antibaryon, flavor oscillation, emission of rarefaction pulses, and/or oppositely oriented mesons.

A lattice of baryonic molecules was constructed in the rotating BEC [21]. Real time dynamics of a few (and many) body system will be an important direction. As real QCD has $SU(3)$ symmetry, our next step will be the confinement of 1/3 quantized vortices in three-component BECs, for which a baryon was constructed numerically in Ref. [30, 31]. While we have shown confinement of charged bosons, the recently highlighted duality between vortices and fermions [32] may provide simulation of QCD with quarks (as fermions).

Acknowledgments This work is supported by

the Ministry of Education, Culture, Sports, Science (MEXT)-Supported Program for the Strategic Research Foundation at Private Universities "Topological Science" (Grant No. S1511006). This work is also supported in part by the Japan Society for the Promotion of Science (JSPS) Grant-in-Aid for Scientific Research (KAKENHI) Grant Numbers (26800119 (M. E.) and 16H03984 (M. E. and M. N.)). The work of M. N. is also supported in part by a Grant-in-Aid for Scientific Research on Innovative Areas "Topological Materials Science" (KAKENHI Grant No. 15H05855) and "Nuclear Matter in Neutron Stars Investigated by Experiments and Astronomical Observations" (KAKENHI Grant No. 15H00841) from the MEXT of Japan.

Appendix A: Numerical details

The baryonic molecule for $g_{12} > 0$ at the equilibrium is static because the inter-vortex repulsion is canceled by the confinement force by the soliton. The equilibrium distance R_0 depends on the Rabi coupling η as shown in Fig. 5. As expected, the baryon shrinks as we increase the Rabi frequency η since the soliton tension is proportional to $\sqrt{\eta}$.

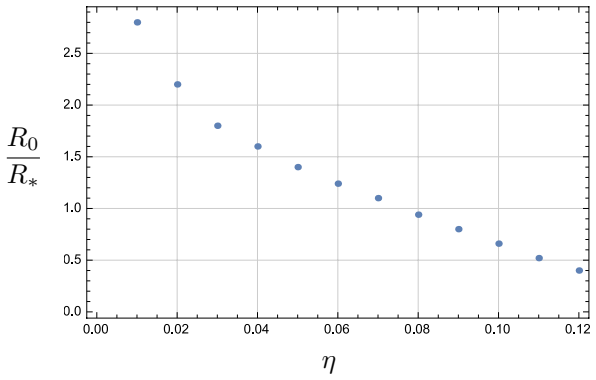

FIG. 5. The equilibrium size R_0 of the baryonic molecule (ud) as function of η. The couplings are chosen as $u = 2u_{12} = 1$.

Once the size of baryon deviates from the equilibrium R_0, it starts to rotate, since the interaction is repulsive (attractive) for $R < R_0$ ($R > R_0$). Let us show several examples with three different sizes i) $R < R_0$, ii) $R = R_0$ and iii) $R > R_0$. Fig. 6 shows typical time evolutions of the baryonic molecules. As can be clearly seen, the size of molecule affects the rotation. The baryon of $R < R_0$ ($R > R_0$) rotates counterclockwise (clockwise). When the molecule size is sufficiently large as $R > R_*$ (but less than the critical length R_c), the soliton tension dominates the inter-vortex force. The rotation period $\mathcal{T}$ of a baryonic molecule is asymptotically given by $\mathcal{T} \to \frac{\pi^2}{4\alpha\sqrt{\eta}}\rho$. We numerically confirm that $\mathcal{T}$ indeed approaches the asymptotic behavior as shown in Fig. 7(a).

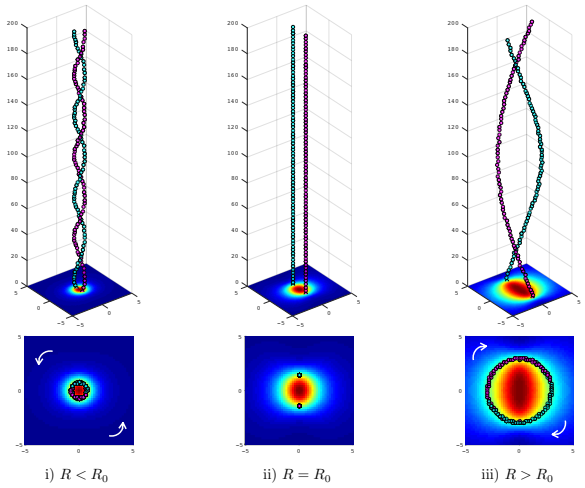

FIG. 6. Typical motions of the ud baryon with the separation i) $R < R_0$, ii) $R = R_0$, and iii) $R > R_0$ with $R_0 = 2.8R_*$. The density plots at the bottom of the upper figures show the Rabi potential density V_R, and the magenta (cyan) makers indicate the position of u vortex (d vortex) from $\tau = 0$ to 200. $u = 2u_{12} = 1$ and $\eta = 0.01$. The figures at the second row are the upper figures seen from the top.

On the other hand, a mesonic molecule moves at a constant velocity. The velocity of a mesonic molecule is asymptotically given by $\mathcal{V} \to \frac{8\alpha\sqrt{\eta}}{\pi}$. Indeed, $\mathcal{V}$ asymptotically approaches to the asymptotic value as R being increased, as can be seen in Fig. 7(b).

When we initially set the size of molecule longer than the critical size R_c, the molecule breaks up with pair creation of vortex and anti-vortex. The phases of Ψ_1 and Ψ_2 clearly show a pair creation phenomenon, as in Fig. 8, in which fragmentation of a long baryon ud ($R_{\rm ini} = 24R_*$) is shown. From this figure, we observe that two pairs, $u\bar{u}$ and $d\bar{d}$, are dynamically created and the soliton is chopped. As a consequence, the initial long ud baryon splits up into three short molecules: two short ud baryons and a semi-long anti-baryon $\bar{d}\bar{u}$. Thus, the baryon number is preserved under this process.

When we put a longer baryon ($R_{\rm ini} = 44R_*$) at initial time, it splits up into five small pieces as shown in Fig. 9(top). Fragmentation occurs in multifolds. Initially, the very long ud baryon releases two short ud baryons from its edges remaining a long anti-baryon ($\bar{d}\bar{u}$) at center as $ud \to ud + \bar{d}\bar{u} + ud$. Soon after the first fragmentation, the two short anti-baryons are separated from the long anti-baryon, leaving another ud baryon at the center as $ud + \bar{d}\bar{u} + ud + \bar{d}\bar{u} + ud$. Then the three baryons rotate clockwise and the two anti-baryons rotate counterclockwise. After a while the configuration becomes $ud + \bar{u}\bar{d} + du + \bar{u}\bar{d} + ud$, and then the three molecules inside coalesce back into a long anti-baryon as $ud + \bar{u}\bar{d} + ud$. Finally, the long anti-baryon $\bar{u}\bar{d}$ at the center again breaks up into the five pieces as $ud + \bar{u}\bar{d} + du + \bar{u}\bar{d} + ud$. The

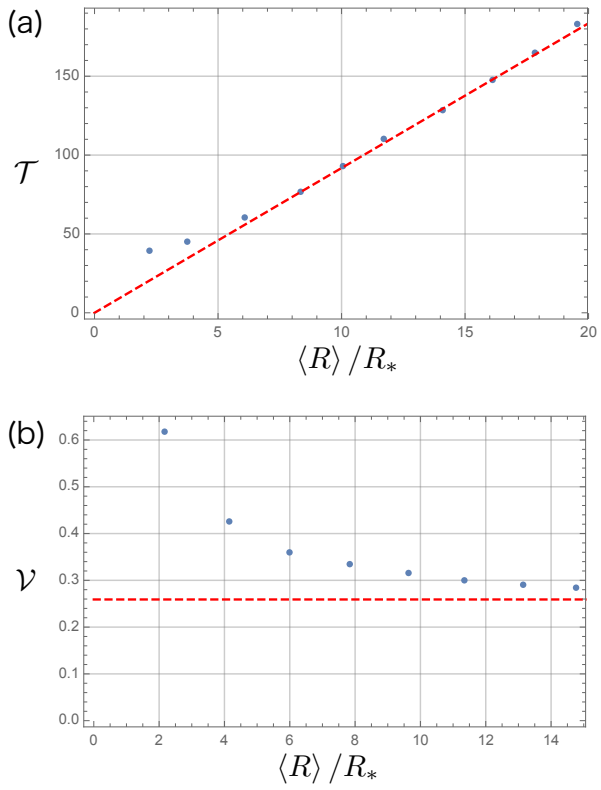

FIG. 7. (a) The period $\mathcal{T}$ of precession of ud as a function of the mean size $\langle R\rangle$. The dashed line is the asymptotic linear function with $\alpha = 0.85$. (b) The velocity $\mathcal{V}$ of $\bar{u}u$ as a function of the mean size $\langle R\rangle$. The red dashed line corresponds to the asymptotic constant value with $\alpha = 0.91$.

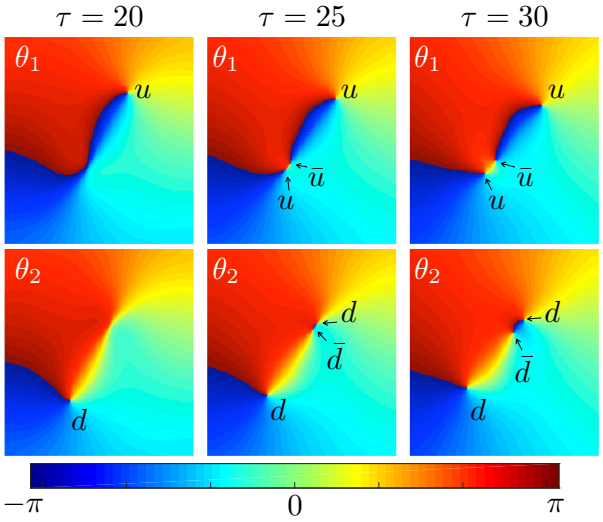

FIG. 8. The phases $\theta_{1,2}$ of $\Psi_{1,2}$ for the motion of Fig. 3. Three snapshots at $\tau = 20, 25, 30$, at which the string fragmentation occurs, are shown. The plot regions are $\vec{y} \in [-20, 20]^2$.

baryon number is preserved at any stage.

Similarly, a very long meson ($R_{\rm ini} = 60R_*$) at initial time breaks up into five or more small molecules as shown in the lower panels of Fig. 9. As for baryons, the fragmentation gradually occurs from the ends of the molecule. Initially, the molecule is $\bar{u}u$ and it splits into $\bar{u}\bar{d}$+$d\bar{d}$+du. At the second stage, it further breaks up into $\bar{u}\bar{d}$+du+$\bar{u}u$+$\bar{u}\bar{d}$+du. Then, it breaks up into six pieces as $\bar{u}\bar{d}$+du+$\bar{u}\bar{d}$+du+$\bar{u}\bar{d}$+du. The meson at the center moves straight downward with showing the flavor oscillations as $\bar{u}u \leftrightarrow \bar{u}\bar{d}$+$du \leftrightarrow \bar{d}\bar{u}$+$ud \leftrightarrow \bar{d}d$.

Appendix B: Baryons and mesons in QCD and BEC

1. Baryons and mesons in $SU(2)$ QCD

Here, we consider $SU(2)$ QCD with two quarks (flavors) u- and d-quarks, and compare states in this theory with those of BECs. In the massless limit, these quarks belong to a doublet of the $SU(2)$ flavor symmetry. Each quark also belongs to a color doublet as $u = (u_r, u_g)$ and $d = (d_r, d_g)$, where r and g are color indices. The color singlet states composed of u- and d-quarks are a triplet baryon and a singlet baryon of the $SU(2)$ flavor symmetry as described below. In detail, the triplet baryon is symmetric in the flavor index and antisymmetric in the color index:

$$\begin{pmatrix} u_r u_g - u_g u_r \\ u_r d_g + d_r u_g - (u_g d_r + d_g u_r) \\ d_r d_g - d_g d_r \end{pmatrix}, \tag{B1}$$

while the singlet baryon is antisymmetric both for the flavor and color indices:

$$u_r d_g - d_r u_g - (u_g d_r - d_g u_r). \tag{B2}$$

Taking into account the fact that spin of quark is 1/2, the triplet should be spin 1, and the singlet should be spin 0.

Next, let us construct mesons. There are triplet meson, given by

$$\begin{pmatrix} u_r \bar{d}_r - u_g \bar{d}_g \\ u_r \bar{u}_r - d_r \bar{d}_r - (u_g \bar{u}_g - d_g \bar{d}_g) \\ d_r \bar{u}_r - d_g \bar{u}_g \end{pmatrix}, \tag{B3}$$

and a singlet meson, given by

$$u_r \bar{u}_r + d_r \bar{d}_r - (u_g \bar{u}_g + d_g \bar{d}_g). \tag{B4}$$

Here, we use the notation $\bar{u}_r = \overline{u_g}$, etc.

2. Baryons and mesons in bosonic $SU(2)$ QCD

Let us consider $SU(2)$ QCD with *bosonic* quarks, since the charged particles concerned in this work are bosons

(spin 0) which are dual to the HQVs in two component BECs. If u and d are bosons, the components of triplet baryon corresponding to Eq. (B1) vanish, while the singlet baryon corresponding to Eq. (B2) survives as $u_r d_g - d_r u_g$. Unlike the baryons, both the triplet and singlet mesons survive even if u and d are bosons. Thus, what we observe in spectra of the bosonic composite states are the singlet baryon, triplet and singlet mesons. The number of the composites is $1 + 3 + 1 = 5$.

3. Baryons and mesons in coherently coupled BECs

Let us compare these with those in coherently coupled BECs which are the ud baryon and $u\bar{u}$ and $d\bar{d}$ as found in this work. In order to obtain the states in BECs, let us truncate the off-diagonal components u_g and d_r in the bosonic QCD. The two component BECs realize only $U(1)$ subgroups of the $SU(2)$ color and $SU(2)$ flavor symmetries. Then, the singlet baryon is

$$u_r d_g, \tag{B5}$$

while the triplet and singlet mesons reduce to

$$\begin{pmatrix} 0 \\ u_r \bar{u}_r + d_g \bar{d}_g \\ 0 \end{pmatrix}, \quad u_r \bar{u}_r - d_g \bar{d}_g, \tag{B6}$$

respectively. They are nothing but what we observed in coherently coupled two-component BECs.

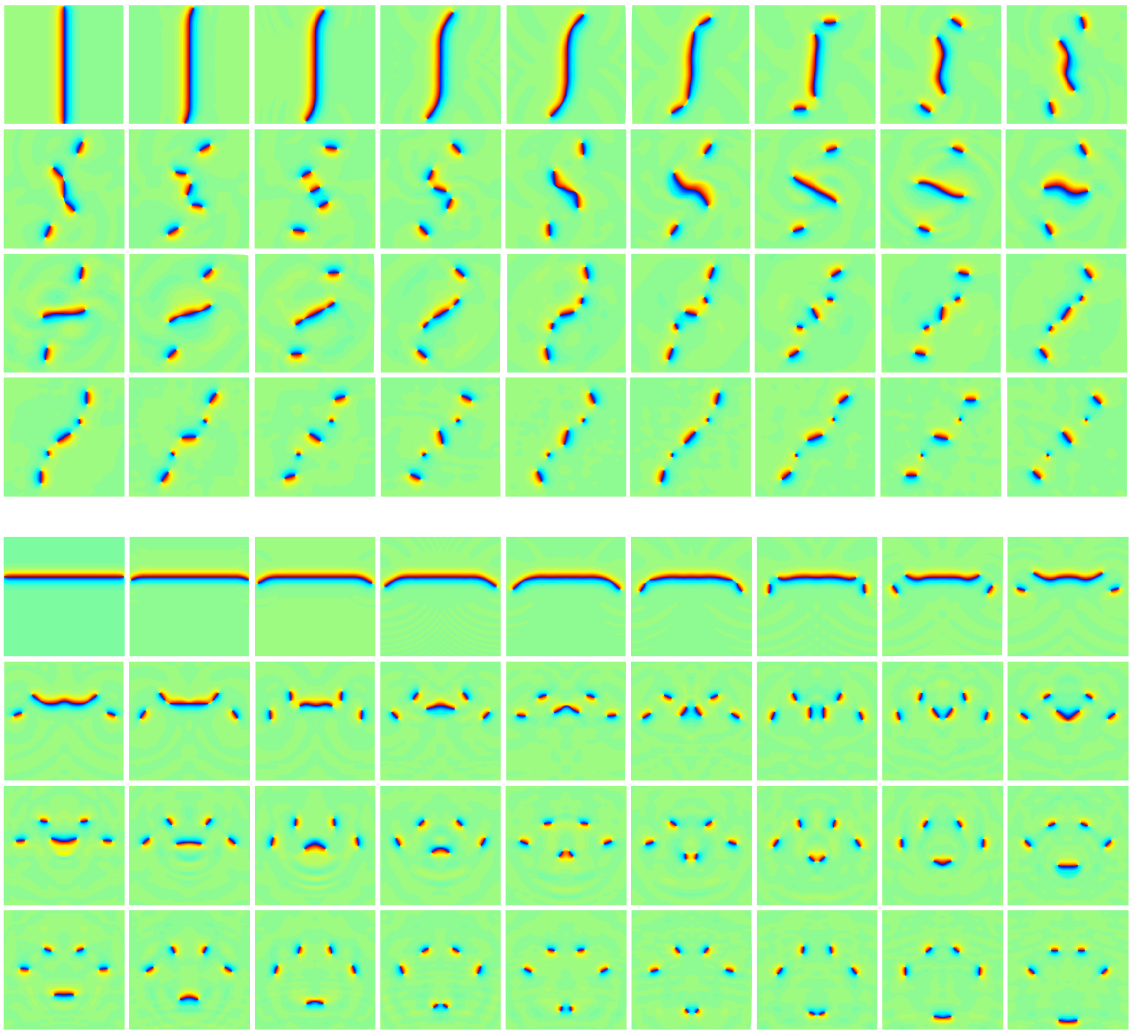

FIG. 9. (The upper panels) A long baryon with $R_{\rm ini} = 44R_*$ breaks up into 3 baryons and 2 anti-baryons. (The lower panels) A long meson with $R_{\rm ini} = 60R_*$ breaks up into 2 baryons, 2 anti-baryons and 1 meson. Real time evolutions for $\tau = 0$ - 175 with a step $\Delta\tau = 5$.

[1] Y. Nambu, Phys. Rev. D **10**, 4262 (1974).
[2] G. 't Hooft, in Proc. of the E.P.S. Int. Conf. on High Energy Physics, Palermo, 23-28 June, 1975 ed. A. Zichichi (Editrice Compositori, Bologna, 1976);
[3] S. Mandelstam, Phys. Rept. **23**, 245 (1976).
[4] A. M. Polyakov, Nucl. Phys. B **120**, 429 (1977).
[5] M. E. Peskin, Annals Phys. **113**, 122 (1978).
[6] C. Dasgupta and B. I. Halperin, Phys. Rev. Lett. **47**, 1556 (1981).
[7] D. H. Lee and M. P. A. Fisher, Phys. Rev. Lett. **63**, 903 (1989).
[8] A. J. Beekman *et.al.*, arXiv:1603.04254 [cond-mat.str-el]
[9] F. Dalfovo, S. Giorgini, L. P. Pitaevskii and S. Stringari, Rev. Mod. Phys. **71**, 463 (1999).
[10] L. Pitaevskii and S. Stringari "Bose-Einstein Condensation and Superfluidity," (Oxford University Press, 2003),
[11] C. J. Pethick, and H. Smith, "Bose-Einstein Condensation in Dilute Gases," (Cambridge University Press, 2008).
[12] D. S. Hall, M. R. Matthews, J. R. Ensher, C. E. Wieman, and E. A. Cornell, Phys. Rev. Lett. **81**, 1539 (1998).
[13] M. R. Matthews, D. S. Hall, D. S. Jin, J. R. Ensher, C. E. Wieman, E. A. Cornell, F. Dalfovo, C. Minniti, and S. Stringari, Phys. Rev. Lett. **81**, 243 (1998); M. R. Matthews, B. P. Anderson, P. C. Haljan, D. S. Hall, M. J. Holland, J. E. Williams, C. E. Wieman, and E. A. Cornell, Phys. Rev. Lett. **83**, 3358 (1999); B. P. Anderson, P. C. Haljan, C. E. Wieman, and E. A. Cornell, Phys. Rev. Lett. **85**, 2857 (2000).
[14] A. L. Fetter, Rev. Mod. Phys. **81**, 647 (2009).
[15] D. V. Freilich, D. M. Bianchi, A. M. Kaufman, T. K. Langin, and D. S. Hall, Science **329**, 1182 (2010); S. Middelkamp, P. J. Torres, P. G. Kevrekidis, D. J. Frantzeskakis, R. Carretero-Gonzalez, P. Schmelcher, D. V. Freilich, D. S. Hall, Phys. Rev. A **84** 011605(R) (2011); R. Navarro, R. Carretero-Gonzalez, P. J. Torres, P. G. Kevrekidis, D. J. Frantzeskakis, M. W. Ray, E. Altuntas, and D. S. Hall, Phys. Rev. Lett. **110**, 225301 (2013).
[16] D. T. Son and M. A. Stephanov, Phys. Rev. A **65**, 063621 (2002)
[17] S. W. Seo, S. Kang, W. J. Kwon, and Y.-I Shin, Phys. Rev. Lett. **115**, 015301 (2015).
[18] K. Kasamatsu, M. Tsubota and M. Ueda, Phys. Rev. Lett. **93**, no. 25, 250406 (2004)
[19] K. Kasamatsu, M. Tsubota and M. Ueda, Int. J. Mod. Phys. **B 19**, 1835 (2005).
[20] J. J. Garcia-Ripoll, V. M. Perez-Garcia, and F. Sols, Phys. Rev. A **66**, 021602 (2002).
[21] M. Cipriani and M. Nitta, Phys. Rev. Lett. **111**, 170401 (2013).
[22] L. Calderaro, A. L. Fetter, P. Massignan, P. Wittek, Phys. Rev. A **95**, no. 1, 023605 (2017).
[23] M. Tylutki, L. P. Pitaevskii, A. Recati and S. Stringari, Phys. Rev. A **93**, no. 4, 043623 (2016).
[24] M. Eto, K. Kasamatsu, M. Nitta, H. Takeuchi and M. Tsubota, Phys. Rev. A **83**, 063603 (2011).
[25] K. Kasamatsu, M. Eto and M. Nitta, Phys. Rev. A **93**, no. 1, 013615 (2016).
[26] A. Usui, H. Takeuchi, Phys. Rev. A **91**, 063635 (2015).
[27] C. Qu, L. P. Pitaevskii, S. Stringari, Phys. Rev. Lett. **116**, 160402 (2016).
[28] C. Qu, M. Tylutki, L. P. Pitaevskii, S. Stringari, arXiv:1609.08499 [cond-mat.quant-gas]
[29] u and d quarks in QCD have a color label as u_a, d_a ($a = r, g$). We identify u_r (d_g) with the θ_1 (θ_2) vortex while u_g and d_r are truncated by the diagonal approximation. The $U(1)$ subgroup of $SU(2)$ color group remains manifest, which we identify $U(1)_R$. See Appendix B for spectra of mesons and baryons constructed by the u_r and d_g only.
[30] M. Eto and M. Nitta, Phys. Rev. A **85**, 053645 (2012); Europhys. Lett. **103**, 60006 (2013).
[31] M. Nitta, M. Eto and M. Cipriani, J. Low. Temp. Phys. **175**, 177 (2013)
[32] D. T. Son, Phys. Rev. X **5**, no. 3, 031027 (2015)